Check for updates

ADVANCING EARTH AND SPACE SCIENCES

JGR Oceans

RESEARCH ARTICLE

10.1029/2023JC020220

Key Points:

- Thermocline diapycnal mixing inferred from a finescale parameterization in the northern Sargasso Sea is enhanced from 1994 to 2019
- Enhanced thermocline diapycnal mixing in the northern Sargasso Sea is due to stronger internal waves excited by intensified winds

Supporting Information:

Supporting Information may be found in the online version of this article.

Correspondence to:

Z. Jing,
jingzhao198763@sina.com

Citation:

Li, Z., Jing, Z., Wu, L., Johnson, R. J., Yang, Z., Song, Z., et al. (2023). Enhanced turbulent diapycnal mixing in the northern Sargasso Sea inferred from a finescale parameterization. *Journal of Geophysical Research: Oceans*, *128*, e2023JC020220. https://doi.org/10.1029/2023JC020220

Received 6 JUL 2023
Accepted 15 NOV 2023

© 2023. American Geophysical Union. All Rights Reserved.

Enhanced Turbulent Diapycnal Mixing in the Northern Sargasso Sea Inferred From a Finescale Parameterization

Zhuoran Li[1], Zhao Jing[1,2], Lixin Wu[1,2], Rodney J. Johnson[3], Zhibin Yang[2], Zhuo Song[2], Zhaohui Chen[1,2], Bolan Gan[1,2], and Xiaohui Ma[1,2]

[1]Key Laboratory of Physical Oceanography and Frontiers Science Center for Deep Ocean Multispheres and Earth System, Ocean University of China, Qingdao, China, [2]Laoshan Laboratory, Qingdao, China, [3]Bermuda Institute of Ocean Sciences, St. George's, Bermuda

Abstract The Sargasso Sea, accommodating marine species and mode water, is highly productive relative to other oligotrophic subtropical regions with intense air-sea carbon and heat exchanges. Turbulent diapycnal mixing regulates these processes and is generally thought to be weakened in a more stratified ocean under anthropogenic forcing. However, by applying a finescale parameterization to long-term hydrographic profiles collected during the Bermuda Atlantic Time-Series Study (BATS), we show that its intensity has become stronger from 1994 to 2019 in the permanent thermocline. The enhanced turbulent diapycnal mixing is mainly attributed to the increase of wind power on internal waves along the Gulf Stream extension. Numerical simulations suggest that stronger internal waves excited along the Gulf Stream extension radiate downward and equatorward, causing enhanced turbulent diapycnal mixing in the northern Sargasso Sea including the BATS station. The findings have important implications for understanding responses of mode water and ecosystem in the Sargasso Sea to anthropogenic forcing.

Plain Language Summary Turbulent mixing contributes to the vertical transport of heat, carbon and nutrients in the ocean, exerting significant effects on the ocean circulations and climate. It is thus important to know how turbulent mixing in the ocean will change under anthropogenic forcing. There is a prevailing thought that turbulent mixing should be weakened under anthropogenic forcing, as the enhanced stratification due to the faster warming in the upper than deeper ocean would hinder the processes generating turbulence. Here, using observation data sampled during the Bermuda Atlantic Time-Series Study (BATS), we find that the turbulent mixing in the permanent thermocline there has increased by 42% over the past three decades. This positive trend is due to stronger wind energy input on internal waves that are gravity waves propagating within the ocean interior rather than on its surface. As these waves radiate downward and equatorward, they transfer their energy into smaller-scale internal waves and eventually break, leading to enhanced turbulent mixing in the northern Sargasso Sea.

1. Introduction

Turbulent diapycnal mixing influences the vertical transport of heat, dissolved gases, nutrients, and pollutants, regulating primary production (A. Gargett & Marra, 2002) and affecting air-sea exchanges of heat and carbon (Gregory, 2000; Sarmiento & Toggweiler, 1984). These functions are particularly true for the Sargasso Sea. The Sargasso Sea is a region where the North Atlantic subtropical mode water (NASTMW) resides. The NASTMW plays a key role in the ocean uptake of atmospheric carbon dioxide (Takahashi et al., 2009) and nutrient cycling (Oka et al., 2015), as it affects climate variabilities through the re-emergence mechanism and many other ways (Hanawa & Sugimoto, 2004; Josey et al., 2018). Providing natural habitats for a variety of marine life (Laffoley et al., 2011), the Sargasso Sea is also an oasis known for its productivity and biodiversity. Both NASTMW and primary production in the Sargasso Sea are strongly regulated by turbulent diapycnal mixing in the upper ocean. Turbulent diapycnal mixing modulates the spread and thickness of NASTMW (Billheimer & Talley, 2013) while promoting air-sea exchanges of heat and carbon (Gregory, 2000; Sarmiento & Toggweiler, 1984). Furthermore, the nutrients pumped upward through turbulent diapycnal mixing fuel the primary production, further enhancing carbon sequestration (A. Gargett & Marra, 2002). Understanding responses of turbulent diapycnal mixing in the upper Sargasso Sea to anthropogenic forcing is of great importance for accurately predicting future climate and ecosystem changes. Yet such responses are still poorly assessed.

10.1029/2023JC020220

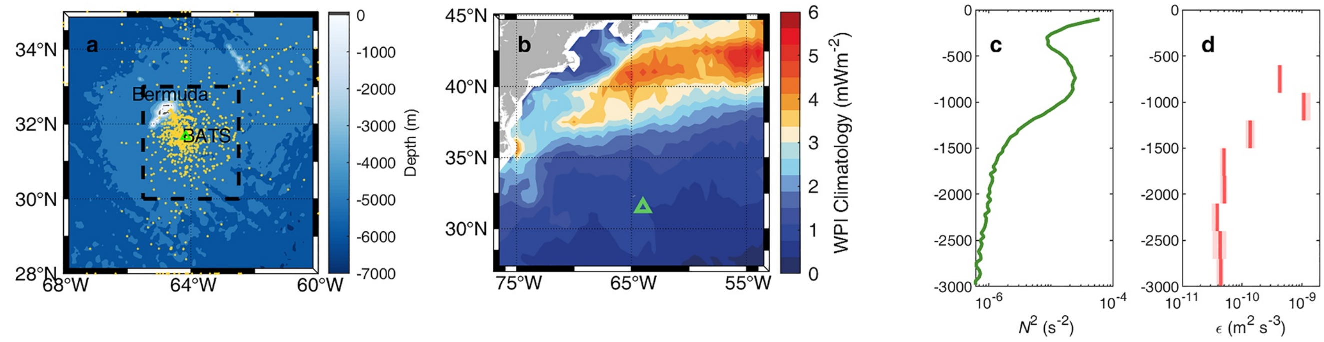

Figure 1. Bathymetrical and hydrographic features of the BATS station. (a) Bathymetry and geographic distribution of the profiles. Yellow points denote the locations of the hydrographic profiles collected from 1994 to 2019. The black dashed line encompasses the region within which the profiles are used in this study. (b) Climatological mean (1994–2018) wind power on near-inertial internal waves W_I in the Northwest Atlantic. (c) and (d) Vertical profiles of climatological mean squared buoyancy frequency N^2 and turbulent kinetic energy dissipation rate ε at the BATS station. The light shading in (d) is 95% confidence interval of the climatological mean ε estimated from a bootstrap method. The green triangle denotes the location of the BATS station.

Highly relevant to and more predictable than the turbulent diapycnal mixing is ocean stratification. A more stratified upper ocean under anthropogenic forcing has been validated by observations (Li et al., 2020; Stevens et al., 2020) and climate model simulations (Fox-Kemper et al., 2021). As intensified stratification acts to inhibit the instability processes generating turbulence (Gargett & Holloway, 1984), an equivalence between intensified stratification and weakened turbulent diapycnal mixing in the upper ocean is widely assumed when studying the impacts of anthropogenic forcing on biological processes (Matear & Hirst, 2003; Moore et al., 2018) and climate (Marzocchi & Jansen, 2017; Oschlies et al., 2018).

However, stratification is not the only factor affecting turbulent diapycnal mixing. Away from the boundary layer, much of turbulent diapycnal mixing occurs through the breaking of internal waves powered primarily by winds and tides (Wunsch & Ferrari, 2004). Existing studies suggest that surface wind fields respond significantly to anthropogenic forcing (Young & Ribal, 2019). Such responses may affect the wind-generated internal waves, making the changes of turbulent diapycnal mixing under anthropogenic forcing more complicated than what should be inferred from the changing stratification alone. The long-term hydrographic profiles collected during the Bermuda Atlantic Time-Series Study (BATS) provide a unique opportunity to test this conjecture.

In this study, by applying a finescale parameterization (Polzin et al., 2014) to the BATS data, we construct the time series of turbulent kinetic energy dissipation rate ε in the permanent thermocline over the past three decades and analyze its controlling factors. The paper is organized as follows. Section 2 details the data and methods. The long-term trend of ε at the BATS station and its attribution to the increased wind power on near-inertial internal waves W_I along the Gulf Stream extension are presented in Section 3. The conclusions of this study are summarized in Section 4 followed by discussion.

2. Data and Methods

2.1. BATS CTD Data

The BATS program is an oceanographic study focusing on the long-term changes of hydrographic and biogeochemical properties of seawater. Since 1988, it has been sampling in the Northwest Atlantic nominally at 31°40'N 64°10'W based on monthly research cruises. During each cruise, continuous profiles of temperature and salinity are collected where the downcast data are used for analysis. After standard processing and corrections, temperature and salinity data are bin-averaged to 2-dbar. By now, about 6,400 profiles have been collected. Here, we only use profiles collected within 30–33°N, 65.5–62.5°W from 1994 to 2019 with a maximal sampling depth greater than 1,000 m, leaving about 3,500 available profiles (Figure 1a). The profiles before 1994 are discarded because a larger rosette was introduced in 1993. This change in the equipment causes an inconsistency in data processing before and after 1994 and may lead to an artificial trend when estimating turbulent diapycnal mixing. After 2019, the data become discontinuous in time, making it difficult to compute the trend.

21699291, 2023, 12, Downloaded from https://agupubs.onlinelibrary.wiley.com/doi/10.1029/2023JC020220 by Ocean University Of China, Wiley Online Library on [18/12/2023]. See the Terms and Conditions (https://onlinelibrary.wiley.com/terms-and-conditions) on Wiley Online Library for rules of use; OA articles are governed by the applicable Creative Commons License

21699291, 2023, 12, Downloaded from https://agupubs.onlinelibrary.wiley.com/doi/10.1029/2023JC020220 by Ocean University Of China, Wiley Online Library on [18/12/2023]. See the Terms and Conditions (https://onlinelibrary.wiley.com/terms-and-conditions) on Wiley Online Library for rules of use; OA articles are governed by the applicable Creative Commons License

2.2. Finescale Parameterization

Based on the idea that weakly nonlinear interactions within a well-developed sea of internal waves act to steadily transport energy from the large (vertical) scales at which they are generated, to the small scales where waves break due to shear or convective instabilities, ε can be expressed in terms of the finescale strain as (Kunze et al., 2006):

$$\varepsilon = \varepsilon_0 \frac{\overline{N}^2}{N_0^2} \frac{<\xi_z^2>^2}{_{\mathrm{GM}}<\xi_z^2>^2} h_2(R_\omega) j\left(f/\overline{N}\right) \tag{1}$$

where $\varepsilon_0 = 6.7 \times 10^{-10} m^2 s^{-3}$, $N_0 = 5.2 \times 10^{-3} rad \cdot s^{-1}$, N^2 is the squared buoyancy frequency, $\overline{N}$ is the vertical mean buoyancy frequency, $_{\mathrm{GM}} < \xi_z^2 >$ is the strain variance from the Garrett-Munk model spectrum (Gregg & Kunze, 1991), and $<\xi_z^2>$ is the observed strain variance. The terms $j\left(f/\overline{N}\right)$ and $h_2(R_\omega)$ are defined as

$$j\left(f/\overline{N}\right) = \frac{f \operatorname{acosh}\left(\overline{N}/f\right)}{f_{30} \operatorname{acosh}(N_0/f_{30})} \tag{2}$$

$$h_2(R_\omega) = \frac{1}{6\sqrt{2}} \frac{R_\omega(R_\omega + 1)}{\sqrt{R_\omega - 1}} \tag{3}$$

where $f_{30} = f(30°)$ and R_ω represents shear/strain variance ratio (fixed at 3 following Whalen et al. (2015)).

All profiles are broken into 300-m segments to evaluate the strain spectra and then the segment-averaged $<\xi_z^2>^2/_{\mathrm{GM}} < \xi_z^2>^2$ and ε (see Jing and Wu (2013) for detailed procedures). The strain spectra may be contaminated due to strong depth variability in the background stratification N^2 (Kunze et al., 2006). Thus, the shallowest two segments, that is, 0–300 m and 300–600 m, are discarded due to the rapid variation of N^2 with depth (Figure 1c).

For the annual mean ε, we first compute the monthly mean ε that is further averaged to obtain the annual mean value. This avoids aliasing of the annual mean by the seasonal cycle as profiles in some years are not evenly distributed among different months. Following Whalen et al. (2015), both the monthly mean and annual mean are computed as the arithmetic mean. We note that the probability distribution of ε estimated from individual hydrographic profiles is far from normal but resembles a positively skewed log-normal distribution (see Figure S1 in Supporting Information S1). In this case, the arithmetic mean may be more affected by some extremely large values than the geometric mean and median. Nevertheless, computing the annual mean in different ways leads to qualitatively consistent long-term trends of annual mean ε during the past three decades (see Figure S2 in Supporting Information S1).

The confidence interval of annual mean ε can be estimated from a bootstrap method with some preprocessing. First, we estimate a climatological mean seasonal cycle of ε (denoted as ε_c; Figure 2c) and compute the anomaly of ε for the individual profiles as $\varepsilon' = \varepsilon - \varepsilon_c$. Then a bootstrap method is applied to ε' during each year to estimate the confidence interval of the annual mean ε'. Finally, this confidence interval is added to the time-mean value of ε_c to get the confidence interval of annual mean ε.

2.3. Wind Power on Near-Inertial Internal Waves

Wind blowing over the sea surface stimulates oceanic near-inertial oscillations in the surface mixed layer. Part of this energy input dissipates in the surface mixed layer, and the remaining radiates into the stratified ocean interior as near-inertial internal waves and plays an important role in powering the turbulent diapycnal mixing (Alford et al., 2016). Here, we use a slab ocean model (Pollard & Millard, 1970) to estimate W_I:

$$\frac{dZ}{dt} + (r + i \cdot f)Z = \frac{T}{H} \tag{4}$$

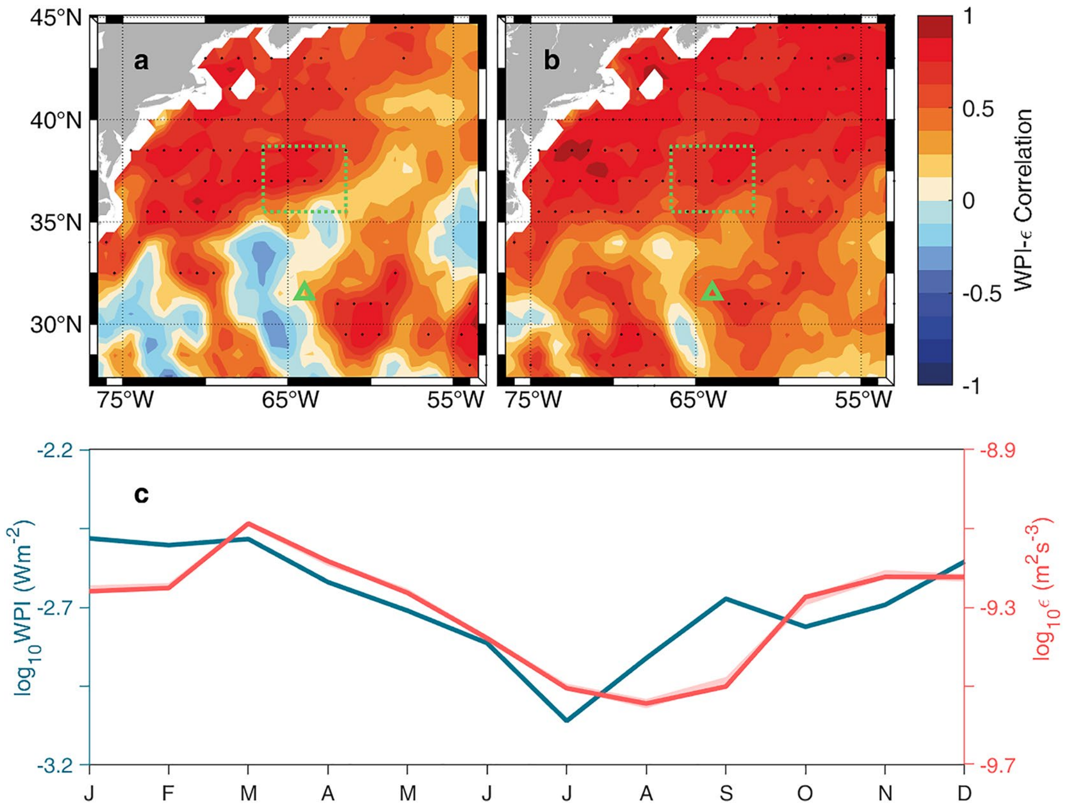

Figure 2. Seasonal cycles of wind power on near-inertial internal waves W_I and turbulent kinetic energy dissipation rate ε in the permanent thermocline at the BATS station and correlation between the two. (a) The simultaneous correlation coefficient between seasonal cycles of ε within 600–900 m at the BATS station and W_I at different locations. (b) Same as (a) but with W_I leading ε by 1 month. Regions where the correlation is significant at 95% confidence level are marked by black dots. The dashed rectangular box (35.5–38.7°N, 61.5–66.5°W) shows the area over which the box-averaged W_I in Figure 3c is calculated. (c) Seasonal cycles of ε within 600–900 m at the BATS station and 1-month-lead W_I averaged within 35.5–38.7°N, 66.5–61.5°W (dashed rectangular box). The light red shading in (c) is 95% confidence interval of the seasonal cycle of ε from a bootstrap method.

where $Z = u + i \cdot v$ is the mixed layer current with $i = \sqrt{-1}$, H is the mixed-layer depth, $T = (\tau_x + i \cdot \tau_y)/\rho$ is the density normalized surface wind stress, and r is the frequency-dependent damping parameter (Alford, 2003). The W_I can be directly computed using the expression:

$$W_I = Z \cdot T \tag{5}$$

The surface wind stress is computed using the 6-hourly 10-m wind vector of ERA-Interim (Dee et al., 2011) spanning from 1979 to 2018. Two other wind data sets, that is, NCEP/NCAR (Kalnay et al., 1996) and Cross-Calibrated Multi-Platform (CCMP) Wind Vector Analysis Product (Atlas et al., 2011) are used for cross-validations.

The mixed layer depth (MLD) is defined as the depth where in situ density changes by 0.03 kg/m^3 compared to that of 10 m using the monthly mean temperature and salinity data from Forecast Ocean Assimilation Model (FOAM) (Blockley et al., 2014) spanning from 1993 to 2018. The monthly mean time series of MLD is used in Equation 4 for computing W_I trend during 1994–2018. As to trend of W_I during 1979–2018, the MLD is fixed as its climatological mean seasonal cycle during 1993–2019, because the MLD data are unavailable before 1993. We find that the variability of MLD on interannual and longer time scales does not impact the robustness of W_I trend (Figure 3c).

2.4. Eddy Kinetic Energy (EKE)

EKE is defined as $^1/_2\left(u'^2_g + v'^2_g\right)$ where (u_g, v_g) are the surface geostrophic velocities and the prime denotes anomalies from the time mean (1994–2019). The values of (u_g, v_g) are derived from sea surface height provided by the SSALTO/Duacs delayed-time 0.25° gridded products (AVISO, 2019).

21699291, 2023, 12, Downloaded from https://agupubs.onlinelibrary.wiley.com/doi/10.1029/2023JC020220 by Ocean University Of China, Wiley Online Library on [18/12/2023]. See the Terms and Conditions (https://onlinelibrary.wiley.com/terms-and-conditions) on Wiley Online Library for rules of use; OA articles are governed by the applicable Creative Commons License

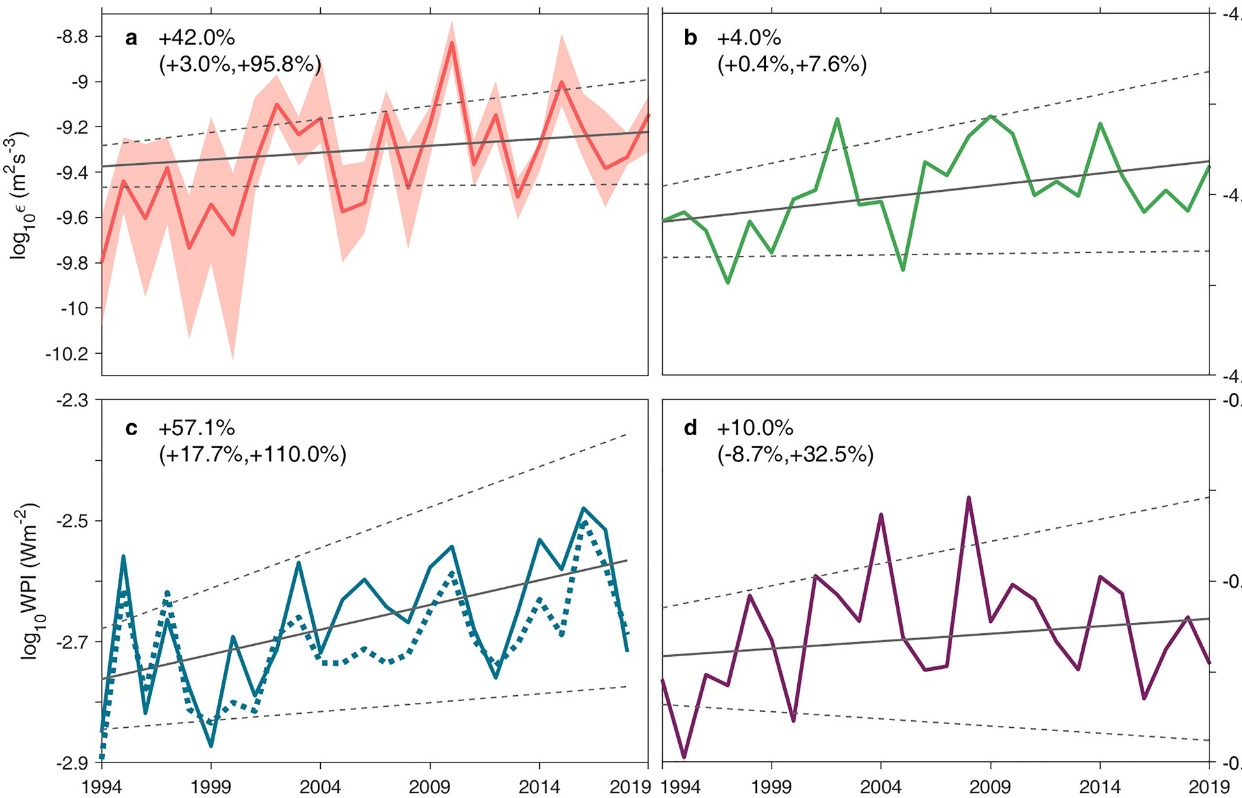

Figure 3. Enhanced turbulent kinetic energy dissipation rate ε from 1994 to 2019 and its controlling factors. (a) Annual mean ε within 600–900 m at the BATS station. The gray solid and dashed lines are the linear fit to the common logarithm of ε and its 95% confidence interval, respectively. (b to d) Same as (a), but for the common logarithm of N^2 at the BATS station, W_I and eddy kinetic energy averaged within 35.5–38.7°N, 66.5–61.5°W. The increase of the corresponding variables during 1994–2019 is denoted in the top-left corner with their 95% confidence intervals in brackets. The dotted thick line in (c) indicates W_I calculated using the climatological mean seasonal cycle of mixed layer depth. The light shading in (a) is the 95% confidence interval of the annual mean ε from a bootstrap method.

2.5. Sea Surface Temperature (SST)

The daily 1/4° Optimum Interpolation Sea Surface Temperature (OISST) v2.1 (Banzon et al., 2020), is used to quantify the SST trend.

2.6. Computation of Long-Term Trend

In this study, the trend for a variable ϕ is computed by performing a linear fit to $\log_{10} \phi$. The slope of such a defined trend quantifies the relative increase of ϕ, facilitating comparisons of trends among different variables.

3. Results

3.1. Enhanced Turbulent Diapycnal Mixing

The BATS station centered around 31°40'N, 64°10'W (Figure 1a) has a hydrographic feature typically observed in the Sargasso Sea. The background stratification given by N^2 exhibits a sharp seasonal thermocline near the surface and a smooth permanent thermocline centered around 800 m below which N^2 decreases monotonically with depth (Figure 1c). The time-mean ε below 600 m estimated from the finescale parameterization attenuates rapidly as the depth increases (Figure 1d). Its value in the permanent thermocline is on the order of $O(10^{-9})$ $m^2\ s^{-3}$, representative of the typical values observed in the Sargasso Sea (Whalen et al., 2015).

The value of ε in the permanent thermocline (600–900 m) at the BATS station exhibits pronounced variability on multiple time scales (Figures 2c and 3a). Consistent with previous studies (Jing & Wu, 2014; Whalen et al., 2012), there is a distinct seasonal cycle with much stronger ε in winter than in summer (Figure 2c). In addition to this well-known seasonal cycle, the new finding here is a positive trend of the annual mean ε (p-value <0.05) over the

21699291, 2023, 12, Downloaded from https://agupubs.onlinelibrary.wiley.com/doi/10.1029/2023JC020220 by Ocean University Of China, Wiley Online Library on [18/12/2023]. See the Terms and Conditions (https://onlinelibrary.wiley.com/terms-and-conditions) on Wiley Online Library for rules of use; OA articles are governed by the applicable Creative Commons License

10.1029/2023JC020220

Table 1
Influences of the Estimation Errors in ε on Its Trend

	Mean value	95% confidence interval
Estimated Trend	+43.0%	(+29.9%, +99.7%)

Note. The confidence interval is evaluated based on 10,000 sensitivity simulations.

past three decades even though the stratification becomes slightly stronger (Figures 3a and 3b). From 1994 to 2019, the value of ε increases by 42%.

The value of ε estimated from the finescale parameterization is unavoidably subject to some uncertainties, which might affect the robustness of its trend. In the open ocean away from rough topography, previous observations revealed that the finescale parameterization can reproduce the value of ε obtained from the microstructure measurements within a factor of 3 (Polzin et al., 1995; Whalen et al., 2015). To examine how errors in the finescale parameterization estimates influence the trend of ε, sensitivity experiments are performed by assuming the ratio of estimated ε for an individual profile to its true value is randomly distributed between 1/3 and 3. The results suggest that the estimation errors do not degrade the robustness of the trend (Table 1). By assuming all the estimation errors are random errors, we tend to overestimate their influences on the trend of ε, as systematic errors do not affect the trend. Therefore, we conclude that the turbulent diapycnal mixing in the permanent thermocline at the BATS station is significantly enhanced over the past three decades and such enhancement is opposite to what would be inferred from the change of stratification alone.

3.2. Increased Wind Power on Near-Inertial Internal Waves

The enhanced thermocline turbulent diapycnal mixing at the BATS station might result from the intensified internal wave fields primarily composed of internal tides and NIWs. There is no synchronous data available for internal wave analysis during the BATS study. However, due to a lack of prominent topographic features within the Sargasso Sea (Figure 1), the conversion from barotropic tides to baroclinic tides is weak in this area (Green & Nycander, 2013; H. L. Simmons et al., 2004). Moreover, a more stratified upper ocean tends to reduce the conversion from barotropic tides to baroclinic tides (Vlasenko et al., 2005). Therefore, the baroclinic tides are unlikely to account for the enhanced thermocline turbulent diapycnal mixing on the long term.

The pronounced seasonal cycle of ε at the BATS station suggests that the wind-generated NIWs play a crucial role in fueling the turbulent diapycnal mixing there, as the intensity of NIWs also exhibits similar seasonality (Alford et al., 2016; Jing & Wu, 2014; Liu et al., 2019). Indeed, there is a tight correlation between the seasonal cycles of ε at the BATS station and W_I to the north when W_I leads ε by 1 month (Figures 2a and 2b). The 1-month lead of W_I results from the slow downward radiation of NIWs whose vertical group velocity is usually tens of meters per day (Alford et al., 2012; Whalen et al., 2012). The tighter association of ε at the BATS station with W_I to the north than local is consistent with the equatorward radiation of NIWs driven by the gradient of planetary vorticity (Garrett, 2001).

The intensity of wind-generated NIWs in the permanent thermocline depends on both the genesis, indicated using W_I, and the efficiency of downward radiation, which will be significantly promoted in the presence of mesoscale eddies (Kunze, 1985; W. R. Young & Jelloul, 1997; Yuan et al., 2022). Previous studies (Joyce et al., 2013; H. Simmons & Alford, 2012) based on mooring data confirm that NIWs in the Sargasso Sea originates from the north in the Gulf Stream extension. This is further supported by the lower correlation of the seasonal cycle of ε to that of the 1-month-lead W_I locally than to the north (Figures 2a and 2b).

The meridional radiation distance for NIWs generated at the sea surface to reach the permanent thermocline can be estimated as: $L = Hc_{gy}/c_{gz}$, where $H = 800$ m is the central depth of permanent thermocline and c_{gy} (c_{gz}) is the meridional (vertical) group velocity. Given large uncertainties in the initial values of c_{gy} and c_{gz} and significant wave refraction due to the varying stratification, planetary vorticity as well as background flow, accurate estimates of c_{gy} and c_{gz} are not available. Nevertheless, an existing literature (Morozov & Velarde, 2008) suggests that c_{gy}/c_{gz} in general ranges from 100 to 1,000. We use this large range as a rule of thumb to estimate possible generation regions for NIWs powering the turbulent diapycnal mixing in the permanent thermocline at the BATS station. This range of radiation (80–800 km) in combination with significant correlation between ε and 1-month-lead W_I (Figure 2b) yields a box covering 35.5–38.7°N to the north of the BATS station.

The annual mean W_I and EKE averaged within box 35.5–38.7°N, 61.5–66.5°W (Figure 2b) are shown in Figures 3c and 3d. The trend of the box-averaged EKE is statistically insignificant, which undermines mesoscale eddies' contribution to the observed secular increase of ε. We also conduct sensitivity experiments by altering the latitude range of the box for the EKE average. Neither the EKE average around the BATS station (30–33°N) nor

21699291, 2023, 12, Downloaded from https://agupubs.onlinelibrary.wiley.com/doi/10.1029/2023JC020220 by Ocean University Of China, Wiley Online Library on [18/12/2023]. See the Terms and Conditions (https://onlinelibrary.wiley.com/terms-and-conditions) on Wiley Online Library for rules of use; OA articles are governed by the applicable Creative Commons License

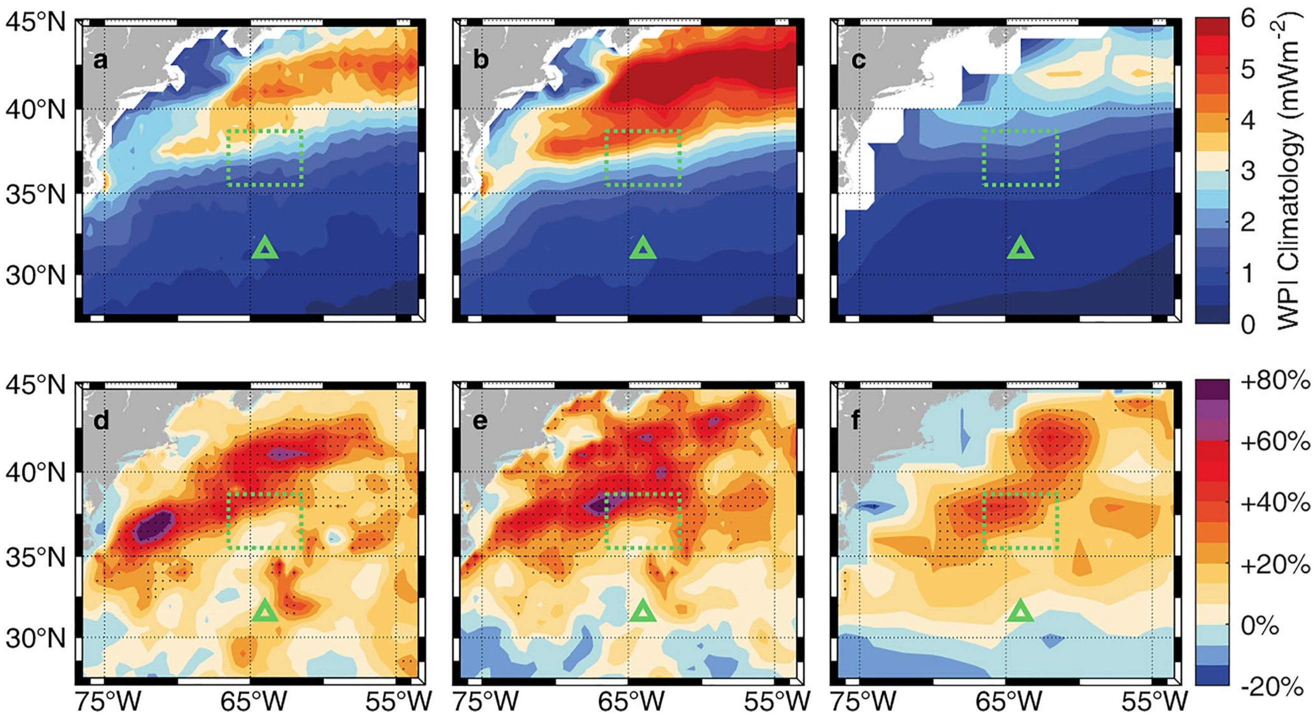

Figure 4. Climatological mean wind power on near-inertial internal waves W_I and its linear trend from different wind products. (a–c) Climatological mean W_I calculated using monthly mean MLD combined with 6-hourly 10-m wind vector from ERA-Interim (1994–2018, 0.5° by 0.5°), CCMP (1994–2018, 0.5° by 0.5°) and NCEP/NCAR (1994–2015, 2.5° by 2.5°), respectively. (d to f) Linear trend of W_I based on the three data sets from (a–c), respectively. Unit here is percentage per decade. Trends significant at 95% confidence level are marked by black dots. The green triangle marks the location of the BATS station. The dashed rectangular box (35.5–38.7°N, 61.5–66.5°W) shows the area over which the box-averaged W_I in Figure 3c is calculated.

that to the north (30–38.7°N) have significant trends (not shown). On the contrary, the box-averaged W_I exhibits significant enhancement over the past three decades. It increases by 57.1% from 1994 to 2018, comparable to that of ε at the BATS station. We remark that using different wind products does not influence the robustness of W_I trend calculated (Figures 4d–4f), although the climatological mean W_I differs substantially among the wind products (Figures 4a–4c) possibly due to the differences in their utilized wind measurements and data processing methods (Kent et al., 2013). This lends further support that the enhanced thermocline turbulent diapycnal mixing at the BATS station over the past three decades is mainly attributed to the increased W_I.

MLD and surface wind stress variance (WSV) are the two variables accountable for W_I (Alford, 2003). It is the long-term change of the latter that dominates the positive trend of box-averaged W_I, as using the climatological mean MLD instead of its monthly mean values to compute W_I has no substantial impact on its trend (Figure 3c). In fact, spatial patterns of W_I and surface WSV trends agree remarkably well with each other (Figures 5a and 5b). Both patterns exhibit pronounced enhancement along the Gulf Stream extension and such enhancement makes a dominant contribution to the trend of box-averaged W_I. Therefore, the secular increase of ε in the permanent thermocline at the BATS station is mainly attributed to the stronger NIWs generated by the intensified sea-surface winds over the Gulf Stream extension.

3.3. Validation Based on Numerical Ocean Simulations

To further substantiate the enhancement of thermocline turbulent diapycnal mixing at the BATS station by the increased W_I along the Gulf Stream extension, two numerical simulations based on an eddy-resolving ocean model (Jamet et al., 2019) are conducted. The simulations use the Massachusetts Institute of Technology general circulation model (MITgcm) (Marshall et al., 1997) with a horizontal resolution of 1/12° and 46 vertical levels spacing from 6 m near the sea surface to 250 at depth. It covers the domain 20°S–55°N, 98°W–14°E, with the open boundary conditions prescribed every 5 days at the north and south boundaries and Strait of Gibraltar. The initial and boundary conditions are derived from a global NEMO simulation ORCA12.L46-MJM88 (Molines et al., 2014). The hourly atmospheric forcings are derived from DRAKKAR Forcing Set (DFS) 4.4

21699291, 2023, 12, Downloaded from https://agupubs.onlinelibrary.wiley.com/doi/10.1029/2023JC020220 by Ocean University Of China, Wiley Online Library on [18/12/2023]. See the Terms and Conditions (https://onlinelibrary.wiley.com/terms-and-conditions) on Wiley Online Library for rules of use; OA articles are governed by the applicable Creative Commons License

21699291, 2023, 12, Downloaded from https://agupubs.onlinelibrary.wiley.com/doi/10.1029/2023JC020220 by Ocean University Of China, Wiley Online Library on [18/12/2023]. See the Terms and Conditions (https://onlinelibrary.wiley.com/terms-and-conditions) on Wiley Online Library for rules of use; OA articles are governed by the applicable Creative Commons License

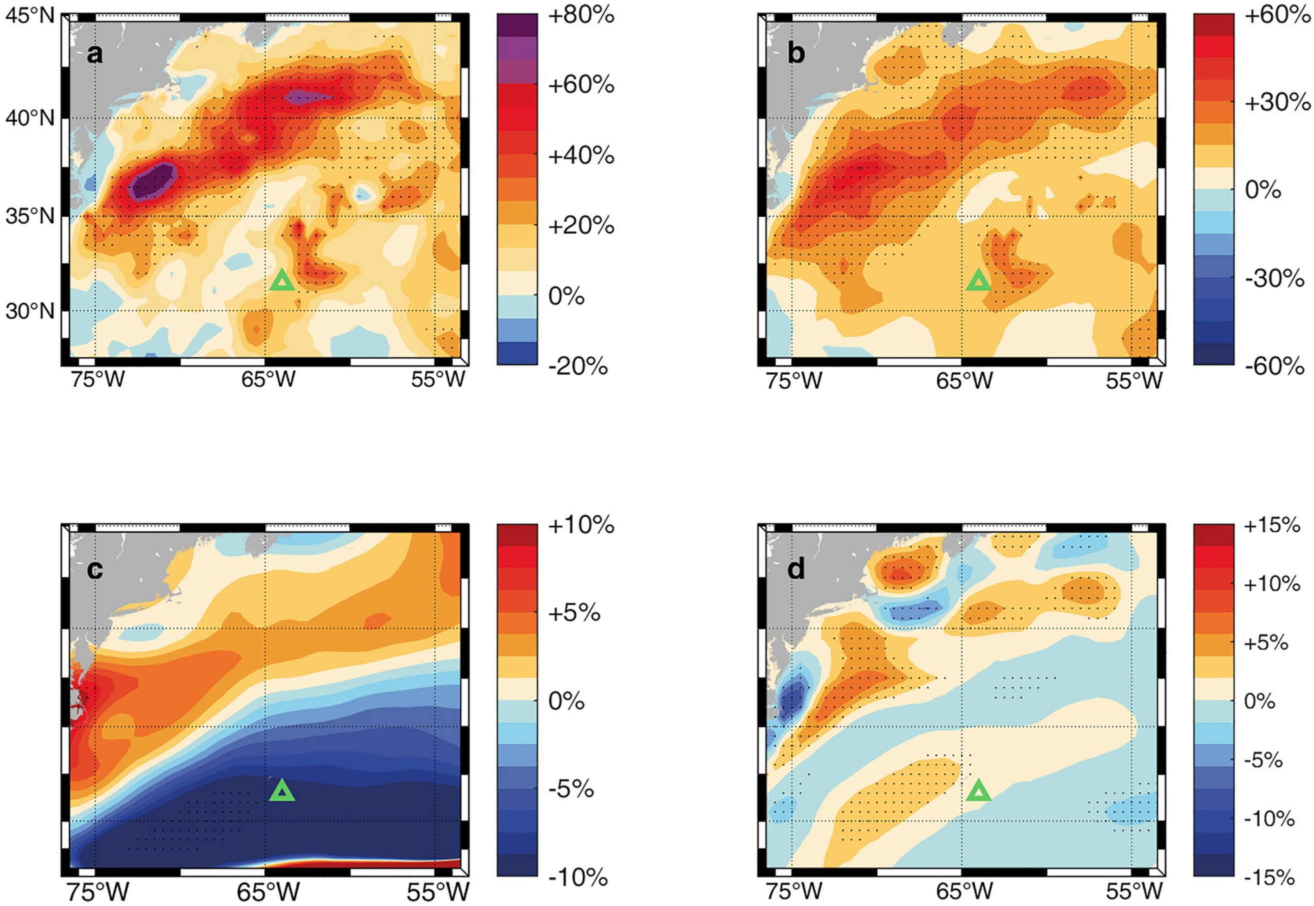

Figure 5. Trends of atmospheric variables during 1994–2018 in the Northwest Atlantic. (a–d) Trends of the common logarithm of W_I, surface wind stress variance (WSV), 850 hPa wind variance, and atmospheric boundary layer height (ABLH) from 1994 to 2018, respectively. Unit here is percentage per decade. Trends significant at 95% confidence level are marked by black dots. The green triangle marks the BATS station.

for 2-m air humidity, 10-m wind vectors, shortwave and longwave radiation and from DFS5.2 for precipitation (Brodeau et al., 2010; Molines et al., 2014) using a boundary layer model named Cheap Atmospheric Mixed Layer (CheapAML; Deremble et al., 2013). The model is initialized in 1958 and run continuously until 2012.

The first simulation (denoted as the CTRL simulation) uses the present-day wind forcing. Although the model simulates the ocean circulations and stratification in the North Atlantic reasonably well (Jamet et al., 2019, 2020), it underestimates W_I along the Gulf Stream extension (Figure S4a in Supporting Information S1; Liu et al., 2019). To remedy this issue, the CTRL simulation is restarted from 31 December 2001 and run until 31 December 2006 with the surface wind forcing replaced by the ERA-Interim. The W_I in the CTRL simulation is stronger and shows better agreement with the observations (Figure S4b in Supporting Information S1; Laffoley et al., 2011).

The wind-amplification simulation (denoted as the WAMP simulation) is the same as the CTRL simulation except for the surface winds. In the WAMP simulation, the wind in the near-inertial band (0.75–1.25 f) is amplified along the Gulf Stream extension by a factor A_{WAMP} from 2002 to 2006 (Figure 6a). To mimic the observed response of W_I to anthropogenic forcing, the value of A_{WAMP} is set as unity everywhere except in the Gulf Stream extension where it is computed as

$$A_{\mathrm{WAMP}} = \sqrt{1.5 \times \beta_{\mathrm{W}_I} \Delta t} \tag{6}$$

where β_{W_I} is the trend of W_I derived from the ERA-Interim (Figure 5a) and Δt is set as 24 years. The symbol of square root arises because W_I is approximately proportional to the near-inertial wind stress variance according to the slab ocean model (Pollard & Millard, 1970). The constant 1.5 is introduced in Equation 6 to enhance the signal-to-noise ratio so that robust statistics for the difference between the WAMP and CTRL

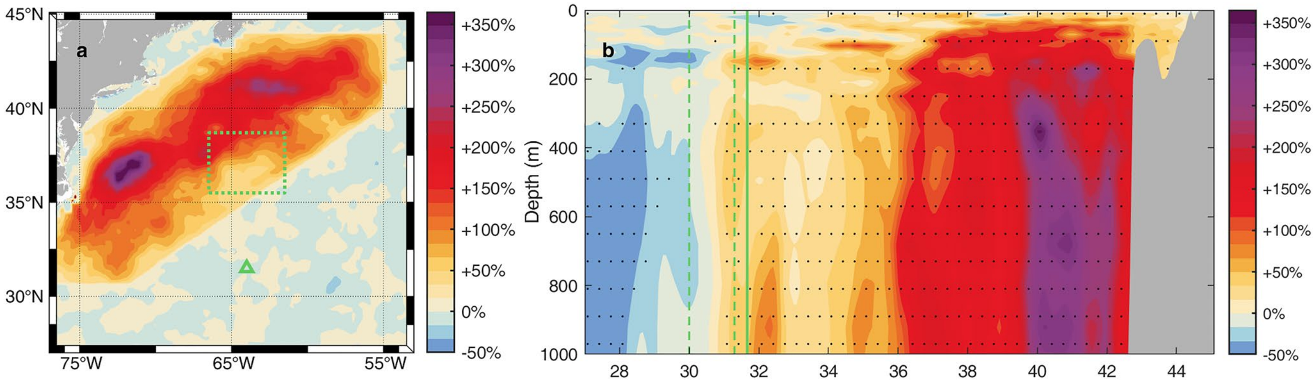

Figure 6. Oceanic response to the enhanced W_I along the Gulf Stream extension simulated by an eddy-resolving ocean numerical model. (a) Difference of the time-mean W_I between the WAMP and CTRL simulations (WAMP-CTRL) normalized by the time-mean W_I in the CTRL simulation. The green triangle marks the BATS station. The dashed rectangular box shows the area over which the box-averaged W_I is calculated. (b) Same as (a) but for the time-mean vertical shear variance of near-inertial internal waves S_I^2 zonally averaged within 66.5–61.5°W. Differences significant at 95% confidence level are marked by black dots. The green solid line marks the location of the BATS station. The southern vicinity (30–31.3° N) of the BATS station is bounded by the two green dashed lines.

simulations can be obtained without running the model for a too long period. It should be noted that the comparison between the WAMP and CTRL simulations is aimed to examine whether the enhanced W_I over the Gulf Stream extension is able to qualitatively intensify the NIWs in the permanent thermocline at the BATS station rather than to derive a quantitative relationship between changes of W_I and turbulent diapycnal mixing.

Figure 6b displays the difference of vertical shear variance of NIWs (denoted as S_I^2) zonally averaged within 66.5–61.5°W between the CTRL and WAMP simulations. The S_I^2, a proxy for the turbulent diapycnal mixing furnished by NIWs, is stronger in the WAMP simulation as a result of increased W_I. The enhanced S_I^2 does not only occur in the surface Gulf Stream extension but also extends equatorward and downward to the permanent thermocline of the BATS station. This provides further evidence that the increased W_I along the Gulf Stream extension could intensify the thermocline turbulent diapycnal mixing at the BATS station via the radiation of NIWs.

It should be noted that the hydrographic profiles analyzed in this study were not exactly collected at the BATS station but in its vicinity within 30–33°N, 65.5–62.5°W (Figure 1a). The ocean simulations suggest that the enhanced S_I^2 by increased W_I along the Gulf Stream extension is more evident to the north of the BATS station, whereas the change of S_I^2 to the south of the BATS station becomes insignificant (Figure 6b). We recompute the time series of ε based on the profiles collected in the southern vicinity (30–31.3°N) of the BATS station. Consistent with the results of ocean simulations, the trend of recomputed ε becomes insignificant (Figure 7). This consistency between the observation and numerical simulations suggests that the increased W_I along the Gulf Stream extension should only enhance the turbulent diapycnal mixing in the northern Sargasso Sea, that is, nearby and to the north of the BATS station.

4. Conclusions and Discussion

By applying a finescale parameterization to monthly CTD profiles from the BATS study, we report a significant long-term increase of ε in the permanent thermocline by 42% from 1994 to 2019 despite the intensified stratification. Further analysis in combination with numerical ocean simulations narrows down the origin of this increase to be the intensified NIWs stimulated by stronger winds over the Gulf Stream extension. The three-decade records of turbulent diapycnal mixing make it difficult to disentangle the anthropogenic effects from natural variabilities on similar time scales, but longer time series (1979–2018) of atmosphere reanalysis products are available and can be used to infer the response of turbulent diapycnal mixing to anthropogenic forcing. It is found that the spatial patterns of surface WSV and W_I trends along the Gulf Stream extension during 1979–2018 are similar to those during 1994–2018 (Figure S3 in Supporting Information S1). This lends support that observed trends of ε and W_I are likely to be the response to anthropogenic forcing.

21699291, 2023, 12, Downloaded from https://agupubs.onlinelibrary.wiley.com/doi/10.1029/2023JC020220 by Ocean University Of China, Wiley Online Library on [18/12/2023]. See the Terms and Conditions (https://onlinelibrary.wiley.com/terms-and-conditions) on Wiley Online Library for rules of use; OA articles are governed by the applicable Creative Commons License

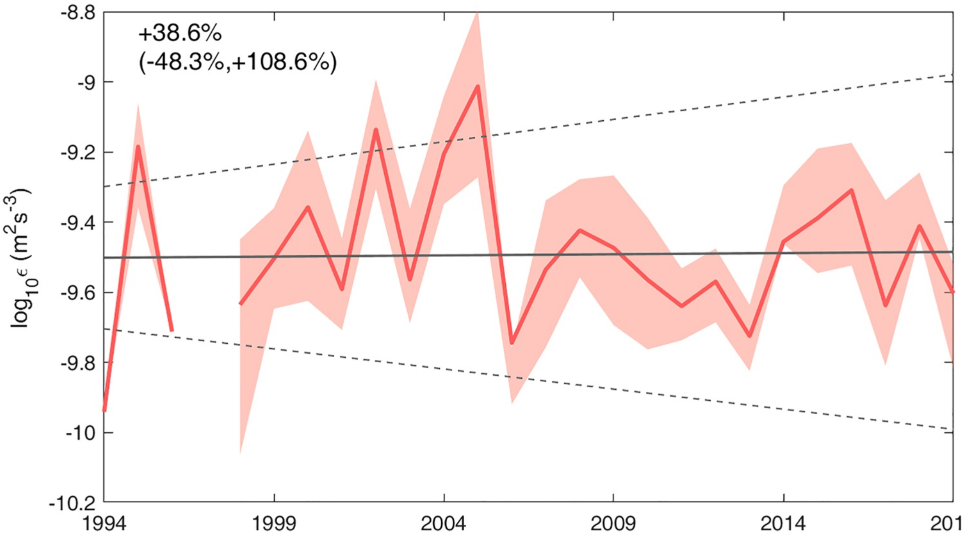

Figure 7. Annual mean ε within 600–900 m estimated based on the hydrographic profiles collected in the southern vicinity (30–31.3°N) of the BATS station. The gray solid line is the linear fit to the common logarithm of ε with the gray dashed lines indicating its 95% confidence interval. The increase of ε in the southern vicinity during 1994–2019 is denoted in the top-left corner with the 95% confidence intervals in the brackets. The light shading represents 95% confidence interval of annual mean values from a bootstrap method.

So far, the mechanisms for the enhanced surface WSV in the Gulf Stream extension remain unclear. The wind variance in the free atmosphere (i.e., at 850 hPa) does not show a similar trend pattern as the surface WSV (Figure 5c), suggesting that the positive trend of surface WSV along the Gulf Stream extension cannot be ascribed to the secular change of atmosphere circulations or synoptic variabilities. Instead, the frontal-scale air-sea interactions seem to provide a more plausible explanation of the enhanced surface WSV (Small et al., 2008; Wallace et al., 1989). It has been well recognized that there is accelerated sea surface warming in the western boundary current extensions under anthropogenic forcing (Wu et al., 2012). This rapid sea surface warming may destabilize the overlying atmosphere and enhance the downward momentum transfer through the vertical mixing mechanism (Small et al., 2008). Indeed, the atmospheric boundary layer height (ABLH) along the Gulf Stream extension rises by more than 20% over 1994–2018 (Figure 5d), lending support to this argument. However, the role of frontal-scale air-sea interaction in enhancing the surface WSV along the Gulf Stream extension should be treated as suggestive rather than definitive.

Findings in this study suggest that the change of turbulent diapycnal mixing under anthropogenic forcing is complicated and can be different from what is inferred from the change of stratification alone. Long-term hydrographic measurements covering the global ocean are thus essential for a comprehensive knowledge of how turbulent diapycnal mixing responds to anthropogenic forcing. This is beyond what shipboard or mooring measurements have to offer. Profiling floats like Argos may provide a promising solution to this issue due to their relatively low costs and long sustainability. Finally, there is a caveat that the long-term trend of ε in this study is not estimated from microstructure measurements but inferred from a finescale parameterization. Although a wide usage of microstructure measurements is far from being achievable due to their high cost, they are necessary for validating and refining the estimates from finescale parameterizations.

Data Availability Statement

All data used in this manuscript are publicly available. The CTD data (Bates & Johnson, 2023) are provided by the Bermuda Institute of Ocean Sciences and available via https://www.bco-dmo.org/dataset/3918. The ERA-Interim data (Dee et al., 2011) are available via https://apps.ecmwf.int/archive-catalogue/?type=an&class=ei&stream=oper&expver=1. The NCEP/NCAR data (Kalnay et al., 1996) via https://psl.noaa.gov/data/gridded/data.ncep.reanalysis.html. The CCMP data (Atlas et al., 2011) via https://data.remss.com/ccmp/v02.0/. The AVISO data (AVISO, 2019) via https://data.marine.copernicus.eu/product/SEALEVEL_GLO_PHY_L4_MY_008_047/services. The OISST data (Banzon et al., 2020) via https://psl.noaa.gov/data/gridded/data.noaa.

21699291, 2023, 12, Downloaded from https://agupubs.onlinelibrary.wiley.com/doi/10.1029/2023JC020220 by Ocean University Of China, Wiley Online Library on [18/12/2023]. See the Terms and Conditions (https://onlinelibrary.wiley.com/terms-and-conditions) on Wiley Online Library for rules of use; OA articles are governed by the applicable Creative Commons License

oisst.v2.html. The FOAM data (Blockley et al., 2014) via https://data.marine.copernicus.eu/product/GLOBAL_REANALYSIS_PHY_001_031/description. The ChaOcean MITgcm code used and data files for re-run can be found at https://github.com/quentinjamet/chaocean. The MatlabR2021b is used for plotting, the software can be downloaded via https://ww2.mathworks.cn/products/new_products/release2021b.html.

Acknowledgments
This research is supported by Marine S&T Fund of Shandong Province for Laoshan Laboratory (No. LSKJ202202502) and Taishan Scholar Funds (tsqn201909052). We thank the Bermuda Institute of Ocean Science for providing the BATS data.

References

Alford, M. H. (2003). Improved global maps and 54-year history of wind-work on ocean inertial motions. *Geophysical Research Letters*, *30*(8), 1424. https://doi.org/10.1029/2002GL016614

Alford, M. H., Cronin, M. F., & Klymak, J. M. (2012). Annual cycle and depth penetration of wind-generated near-inertial internal waves at Ocean Station Papa in the northeast Pacific. *Journal of Physical Oceanography*, *42*(6), 889–909. https://doi.org/10.1175/JPO-D-11-092.1

Alford, M. H., MacKinnon, J. A., Simmons, H. L., & Nash, J. D. (2016). Near-inertial internal gravity waves in the ocean. *Annual Review of Marine Science*, *8*(1), 95–123. https://doi.org/10.1146/annurev-marine-010814-015746

Atlas, R., Hoffman, R. N., Ardizzone, J., Leidner, S. M., Jusem, J. C., Smith, D. K., & Gombos, D. (2011). A cross-calibrated, multiplatform ocean surface wind velocity product for meteorological and oceanographic applications [Dataset]. Bulletin of the American Meteorological Society, *92*(2), 157–174. https://doi.org/10.1175/2010BAMS2946.1

AVISO. (2019). Global ocean gridded L4 sea surface heights and derived variables reprocessed 1993 ongoing [Dataset]. E.U Copernicus Marine and Environment Monitoring Service (CMEMS), Marine Data Store (MDS). https://doi.org/10.48670/moi-00148

Banzon, V., Smith, T. M., Steele, M., Huang, B., & Zhang, H.-M. (2020). Improved estimation of proxy sea surface temperature in the Arctic [Dataset]. Journal of Atmospheric and Oceanic Technology, *37*(2), 341–349. https://doi.org/10.1175/JTECH-D-19-0177.1

Bates, N., & Johnson, R. J. (2023). Two decibar-averaged CTD profiles collected at Bermuda Atlantic Time Series sites in the Sargasso Sea ongoing from 1988 (BATS project) ver 5 [Dataset]. Biological and Chemical Oceanography Data Management Office (BCO-DMO). Retrieved from https://www.bco-dmo.org/dataset/3918

Billheimer, S., & Talley, L. D. (2013). Near cessation of eighteen degree water renewal in the western North Atlantic in the warm winter of 2011–2012. *Journal of Geophysical Research: Oceans*, *118*(12), 6838–6853. https://doi.org/10.1002/2013JC009024

Blockley, E. W., Martin, M. J., McLaren, A. J., Ryan, A. G., Waters, J., Lea, D. J., et al. (2014). Recent development of the Met Office operational ocean forecasting system: An overview and assessment of the new Global FOAM forecasts [Dataset]. Geoscientific Model Development, *7*(6), 2613–2638. https://doi.org/10.5194/gmd-7-2613-2014

Brodeau, L., Barnier, B., Treguier, A.-M., Penduff, T., & Gulev, S. (2010). An ERA40-based atmospheric forcing for global ocean circulation models. *Ocean Modelling*, *31*(3), 88–104. https://doi.org/10.1016/j.ocemod.2009.10.005

Dee, D. P., Uppala, S. M., Simmons, A. J., Berrisford, P., Poli, P., Kobayashi, S., et al. (2011). The ERA-Interim reanalysis: Configuration and performance of the data assimilation system [Dataset]. Quarterly Journal of the Royal Meteorological Society, *37*(656), 553–597. https://doi.org/10.1002/qj.828

Deremble, B., Wienders, N., & Dewar, W. K. (2013). CheapAML: A simple, atmospheric boundary layer model for use in ocean-only model calculations. *Monthly Weather Review*, *141*(2), 809–821. https://doi.org/10.1175/MWR-D-11-00254.1

Fox-Kemper, B., Hewitt, H. T., Xiao, C., Aðalgeirsdóttir, G., Drijfhout, S. S., Edwards, T. L., et al. (2021). Ocean, cryosphere, and sea level change. In V. Masson-Delmotte, P. Zhai, A. Pirani, S. L. Connors, C. Péan, S. Berger, et al. (Eds.), *Climate Change 2021: The Physical Science Basis. Contribution of Working Group I to the Sixth Assessment Report of the Intergovernmental Panel on Climate Change* (pp. 1211–1362). Cambridge University Press. https://doi.org/10.1017/9781009157896.001

Gargett, A., & Marra, J. (2002). Effects of upper ocean physical processes on oceanic primary production. *Sea*, *12*, 19–49.

Gargett, A. E., & Holloway, G. (1984). Dissipation and diffusion by internal wave breaking. *Journal of Marine Research*, *42*(1), 15–27. https://doi.org/10.1357/002224084788506158

Garrett, C. (2001). What is the "near-inertial" band and why is it different from the rest of the internal wave spectrum? *Journal of Physical Oceanography*, *31*(4), 10–971. https://doi.org/10.1175/1520-0485(2001)031<0962:witnib>2.0.co;2

Green, J. A. M., & Nycander, J. (2013). A comparison of tidal conversion parameterizations for tidal models. *Journal of Physical Oceanography*, *43*(1), 104–119. https://doi.org/10.1175/JPO-D-12-023.1

Gregg, M. C., & Kunze, E. (1991). Shear and strain in Santa Monica basin. *Journal of Geophysical Research*, *96*(C9), 16709–16719. https://doi.org/10.1029/91JC01385

Gregory, J. M. (2000). Vertical heat transports in the ocean and their effect on time-dependent climate change. *Climate Dynamics*, *16*(7), 501–515. https://doi.org/10.1007/s003820000059

Hanawa, K., & Sugimoto, S. (2004). "Reemergence" areas of winter sea surface temperature anomalies in the world's oceans. *Geophysical Research Letters*, *31*(10), L10303. https://doi.org/10.1029/2004GL019904

Jamet, Q., Dewar, W. K., Wienders, N., & Deremble, B. (2019). Spatiotemporal patterns of chaos in the Atlantic overturning circulation. *Geophysical Research Letters*, *46*(13), 7509–7517. https://doi.org/10.1029/2019GL082552

Jamet, Q., Dewar, W. K., Wienders, N., Deremble, B., Close, S., & Penduff, T. (2020). Locally and remotely forced subtropical AMOC variability: A matter of time scales. *Journal of Climate*, *33*(12), 5155–5172. https://doi.org/10.1175/JCLI-D-19-0844.1

Jing, Z., & Wu, L. (2013). Low-frequency modulation of turbulent diapycnal mixing by anticyclonic eddies Inferred from the HOT Time Series. *Journal of Physical Oceanography*, *43*(4), 824–835. https://doi.org/10.1175/JPO-D-11-0150.1

Jing, Z., & Wu, L. (2014). Intensified diapycnal mixing in the midlatitude western boundary currents. *Scientific Reports*, *4*(1), 7412. https://doi.org/10.1038/srep07412

Josey, S. A., Hirschi, J. J.-M., Sinha, B., Duchez, A., Grist, J. P., & Marsh, R. (2018). The recent Atlantic cold anomaly: Causes, consequences, and related phenomena. *Annual Review of Marine Science*, *10*(1), 475–501. https://doi.org/10.1146/annurev-marine-121916-063102

Joyce, T. M., Toole, J. M., Klein, P., & Thomas, L. N. (2013). A near-inertial mode observed within a Gulf Stream warm-core ring. *Journal of Geophysical Research: Oceans*, *118*(4), 1797–1806. https://doi.org/10.1002/jgrc.20141

Kalnay, E., Kanamitsu, M., Kistler, R., Collins, W., Deaven, D., Gandin, L., et al. (1996). The NCEP/NCAR 40-year reanalysis project [Dataset]. American Meteorological Society, *77*(3), 437–471. https://doi.org/10.1175/1520-0477(1996)077<0437:tnyrp>2.0.co;2

Kent, E. C., Fangohr, S., & Berry, D. I. (2013). A comparative assessment of monthly mean wind speed products over the global ocean. *International Journal of Climatology*, *33*(11), 2520–2541. https://doi.org/10.1002/joc.3606

21699291, 2023, 12, Downloaded from https://agupubs.onlinelibrary.wiley.com/doi/10.1029/2023JC020220 by Ocean University Of China, Wiley Online Library on [18/12/2023]. See the Terms and Conditions (https://onlinelibrary.wiley.com/terms-and-conditions) on Wiley Online Library for rules of use; OA articles are governed by the applicable Creative Commons License

10.1029/2023JC020220

Kunze, E. (1985). Near-inertial wave propagation in geostrophic shear. *Journal of Physical Oceanography*, *15*(5), 544–565. https://doi.org/10.1175/1520-0485(1985)015<0544:NIWPIG>2.0.CO;2

Kunze, E., Firing, E., Hummon, J. M., Chereskin, T. K., & Thurnherr, A. M. (2006). Global abyssal mixing inferred from lowered ADCP shear and CTD strain profiles. *Journal of Physical Oceanography*, *36*(8), 1553–1576. https://doi.org/10.1175/JPO2926.1

Laffoley, D. d.'A., Roe, H. S. J., Angel, M. V., Ardron, J., Bates, N. R., Boyd, L. L., et al. (2011). The protection and management of the Sargasso Sea: The golden floating rainforest of the Atlantic ocean: Summary science and supporting evidence case.

Li, G., Cheng, L., Zhu, J., Trenberth, K. E., Mann, M. E., & Abraham, J. P. (2020). Increasing ocean stratification over the past half-century. *Nature Climate Change*, *10*(12), 1116–1123. https://doi.org/10.1038/s41558-020-00918-2

Liu, Y., Jing, Z., & Wu, L. (2019). Wind power on oceanic near-inertial oscillations in the global ocean estimated from surface drifters. *Geophysical Research Letters*, *46*(5), 2647–2653. https://doi.org/10.1029/2018GL081712

Marshall, J., Adcroft, A., Hill, C., Perelman, L., & Heisey, C. (1997). A finite-volume, incompressible Navier Stokes model for studies of the ocean on parallel computers. *Journal of Geophysical Research*, *102*(C3), 5753–5766. https://doi.org/10.1029/96JC02775

Marzocchi, A., & Jansen, M. F. (2017). Connecting Antarctic sea ice to deep-ocean circulation in modern and glacial climate simulations. *Geophysical Research Letters*, *44*(12), 6286–6295. https://doi.org/10.1002/2017GL073936

Matear, R. J., & Hirst, A. C. (2003). Long-term changes in dissolved oxygen concentrations in the ocean caused by protracted global warming. *Global Biogeochemical Cycles*, *17*(4). https://doi.org/10.1029/2002GB001997

Molines, J. M., Barnier, B., Penduff, T., Treguier, A. M., & Le Sommer, J. (2014). ORCA12. L46 climatological and interannual simulations forced with DFS4. 4: GJM02 and MJM88. Drakkar Group Experiment Rep. GDRI-DRAKKAR-2014-03-19 (p. 50).

Moore, J. K., Fu, W., Primeau, F., Britten, G. L., Lindsay, K., Long, M., et al. (2018). Sustained climate warming drives declining marine biological productivity. *Science*, *359*(6380), 1139–1143. https://doi.org/10.1126/science.aao6379

Morozov, E. G., & Velarde, M. G. (2008). Inertial oscillations as deep ocean response to hurricanes. *Journal of Oceanography*, *64*(4), 495–509. https://doi.org/10.1007/s10872-008-0042-0

Oka, E., Qiu, B., Takatani, Y., Enyo, K., Sasano, D., Kosugi, N., et al. (2015). Decadal variability of Subtropical Mode Water subduction and its impact on biogeochemistry. *Journal of Oceanography*, *71*(4), 389–400. https://doi.org/10.1007/s10872-015-0300-x

Oschlies, A., Brandt, P., Stramma, L., & Schmidtko, S. (2018). Drivers and mechanisms of ocean deoxygenation. *Nature Geoscience*, *11*(7), 467–473. https://doi.org/10.1038/s41561-018-0152-2

Pollard, R. T., & Millard, R. C. (1970). Comparison between observed and simulated wind-generated inertial oscillations. *Deep-Sea Research and Oceanographic Abstracts*, *17*(4), 813–821. https://doi.org/10.1016/0011-7471(70)90043-4

Polzin, K. L., Naveira Garabato, A. C., Huussen, T. N., Sloyan, B. M., & Waterman, S. (2014). Finescale parameterizations of turbulent dissipation: Finescale Parameterizations. *Journal of Geophysical Research: Oceans*, *119*(2), 1383–1419. https://doi.org/10.1002/2013JC008979

Polzin, K. L., Toole, J. M., & Schmitt, R. W. (1995). Finescale parameterizations of turbulent dissipation. *Journal of Physical Oceanography*, *25*(3), 306–328. https://doi.org/10.1175/1520-0485(1995)025<0306:fpotd>2.0.co;2

Sarmiento, J. L., & Toggweiler, J. R. (1984). A new model for the role of the oceans in determining atmospheric P CO_2. *Nature*, *308*(5960), 621–624. https://doi.org/10.1038/308621a0

Simmons, H., & Alford, M. (2012). Simulating the long-range swell of internal waves generated by ocean storms. *Oceanography*, *25*(2), 30–41. https://doi.org/10.5670/oceanog.2012.39

Simmons, H. L., Hallberg, R. W., & Arbic, B. K. (2004). Internal wave generation in a global baroclinic tide model. *Deep Sea Research Part II: Topical Studies in Oceanography*, *51*(25), 3043–3068. https://doi.org/10.1016/j.dsr2.2004.09.015

Small, R. J., de Szoeke, S. P., Xie, S. P., O'Neill, L., Seo, H., Song, Q., et al. (2008). Air–sea interaction over ocean fronts and eddies. *Dynamics of Atmospheres and Oceans*, *45*(3–4), 274–319. https://doi.org/10.1016/j.dynatmoce.2008.01.001

Stevens, S. W., Johnson, R. J., Maze, G., & Bates, N. R. (2020). A recent decline in North Atlantic subtropical mode water formation. *Nature Climate Change*, *10*(4), 335–341. https://doi.org/10.1038/s41558-020-0722-3

Takahashi, T., Sutherland, S. C., Wanninkhof, R., Sweeney, C., Feely, R. A., Chipman, D. W., et al. (2009). Climatological mean and decadal change in surface ocean pCO2, and net sea–air CO_2 flux over the global oceans. *Deep Sea Research Part II: Topical Studies in Oceanography*, *56*(8–10), 554–577. https://doi.org/10.1016/j.dsr2.2008.12.009

Vlasenko, V., Stashchuk, N., & Hutter, K. (2005). *Baroclinic tides: Theoretical modeling and observational evidence* (1st ed.). Cambridge University Press. https://doi.org/10.1017/CBO9780511535932

Wallace, J. M., Mitchell, T. P., & Deser, C. (1989). The influence of sea-surface temperature on surface wind in the eastern equatorial Pacific: Seasonal and interannual variability. *Journal of Climate*, *2*(12), 1492–1499. https://doi.org/10.1175/1520-0442(1989)002<1492:TIOSST>2.0.CO;2

Whalen, C. B., MacKinnon, J. A., Talley, L. D., & Waterhouse, A. F. (2015). Estimating the mean diapycnal mixing using a finescale strain parameterization. *Journal of Physical Oceanography*, *45*(4), 1174–1188. https://doi.org/10.1175/JPO-D-14-0167.1

Whalen, C. B., Talley, L. D., & MacKinnon, J. A. (2012). Spatial and temporal variability of global ocean mixing inferred from Argo profiles. *Geophysical Research Letters*, *39*(18), L18612. https://doi.org/10.1029/2012GL053196

Wu, L., Cai, W., Zhang, L., Nakamura, H., Timmermann, A., Joyce, T., et al. (2012). Enhanced warming over the global subtropical western boundary currents. *Nature Climate Change*, *2*(3), 161–166. https://doi.org/10.1038/nclimate1353

Wunsch, C., & Ferrari, R. (2004). Vertical mixing, energy, and the general circulation of the oceans. *Annual Review of Fluid Mechanics*, *36*(1), 281–314. https://doi.org/10.1146/annurev.fluid.36.050802.122121

Young, I. R., & Ribal, A. (2019). Multiplatform evaluation of global trends in wind speed and wave height. *Science*, *364*(6440), 548–552. https://doi.org/10.1126/science.aav9527

Young, W. R., & Jelloul, M. B. (1997). Propagation of near-inertial oscillations through a geostrophic flow. *Journal of Marine Research*, *55*(4), 735–766. https://doi.org/10.1357/0022240973224283

Yuan, M., Song, Z., Jing, Z., Li, Z., & Wu, L. (2022). Distinct roles of global cyclonic and anticyclonic eddies in regulating near-inertial internal waves in the ocean interior. *Frontiers in Marine Science*, *9*. https://doi.org/10.3389/fmars.2023.1134579

21699291, 2023, 12, Downloaded from https://agupubs.onlinelibrary.wiley.com/doi/10.1029/2023JC020220 by Ocean University Of China, Wiley Online Library on [18/12/2023]. See the Terms and Conditions (https://onlinelibrary.wiley.com/terms-and-conditions) on Wiley Online Library for rules of use; OA articles are governed by the applicable Creative Commons License